Low-energy K−-nucleus/nuclei interactions with light nuclei with AMADEUS

Catalina Curceanu
INFN Laboratori Nazionali di Frascati, 00044 Frascati, Italy
On the behalf of the AMADEUS collaboration

ROCKSTAR: Towards a ROadmap of the Crucial measurements of Key observables in Strangeness reactions for neutron sTARs equation of state
9-13 October 2023, ECT - Trento (Italy)*

AMADEUS scientific case

AMADEUS (**A**ntikaonic **M**atter **A**t **D**AΦNE: an **E**xperiment with **U**nravelling **S**pectroscopy) investigates **low-energy K^- absorption in nuclei** with the aim to extract information on:

- K^-N interaction above and below threshold
  - Λ(1405) nature
  - K^-N scattering amplitudes and cross sections
- K^-NN, K^-NNN, K^-NNNN (multi-nucleon) interactions
  - K^--multi nucleon cross sections
  - essential for the determination of K^--nuclei optical potential
  - kaonic bound states
- Hyperon-nucleon/(multi-nucleons) interaction cross sections

DAΦNE the Φ factory

INFN Istituto Nazionale di Fisica Nucleare
LABORATORI NAZIONALI DI FRASCATI

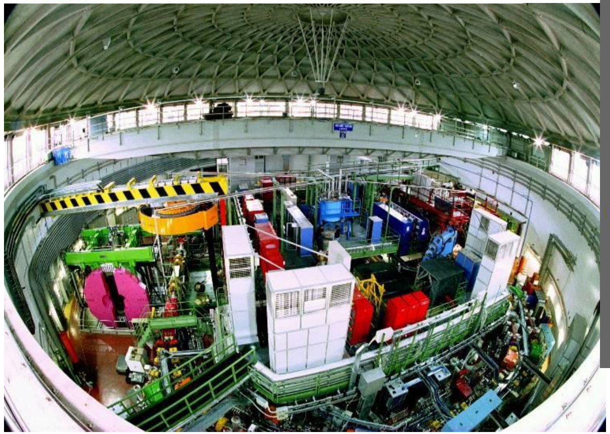

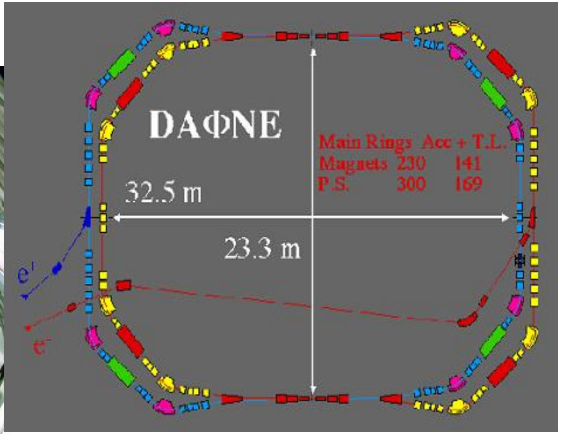

- $e^+ e^-$ at 510 MeV
- φ resonance decays at 49 % in $K^+ K^-$ back to back pair
- Very low momentum (≈ 127 MeV/c) K^- beam

Unique low momentum K^- factory

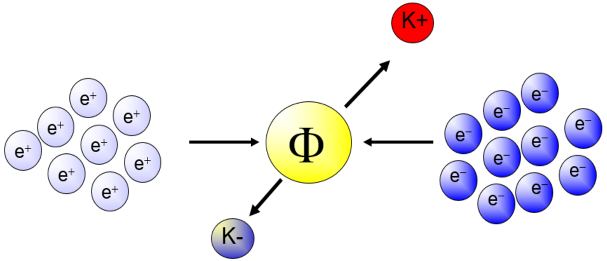

Suitable for low-energy kaon physics:
→ **Kaonic atoms** (**SIDDHARTA-2**)
→ **Kaon-nucleons/nuclei interaction** studies (**AMADEUS**)

LNF - e^+e^- Accelerator Complex

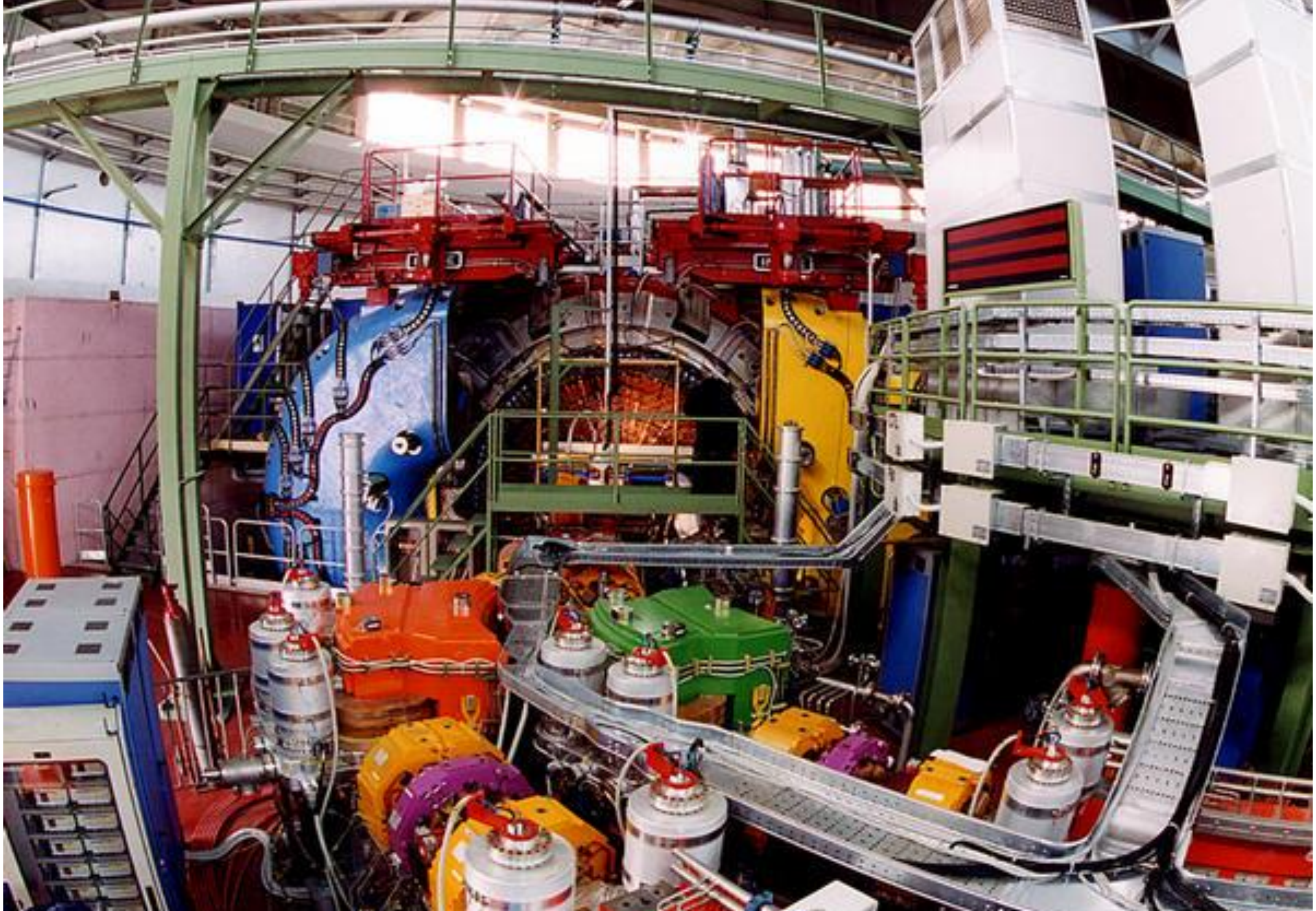

AMADEUS

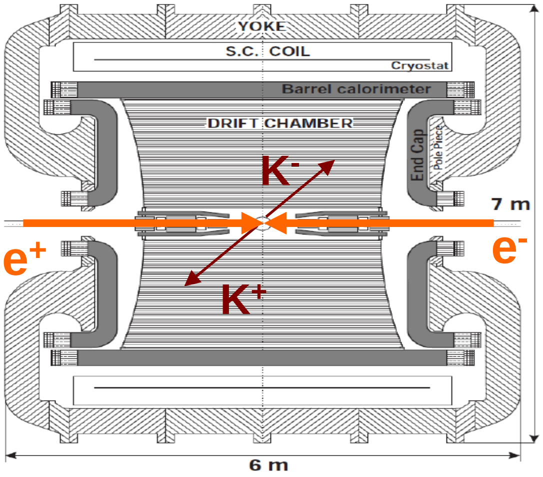

The KLOE detector

Cylindrical drift chamber with a **4π geometry** and electromagnetic calorimeter, **96% acceptance**

- optimized in the energy range of all **charged particles** involved
- **good performance** in detecting **photons and neutrons** checked by kloNe group
  [M. Anelli et al., Nucl Inst. Meth. A 581, 368 (2007)]

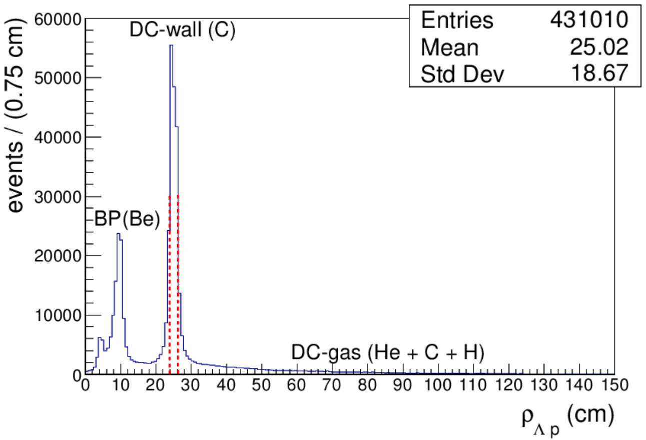

KLOE used as an active target

- DC wall (750 μm C foil , 150 μm Al foil);
- DC gas (90% He, 10% C_4H_{10}).
  +
  pure sample of K^- ^{12}C absorptions at-rest

K^- absorptions at-rest and in-flight

AT-REST

K^- absorbed from atomic orbitals

($p_K \sim 0$ MeV/c)

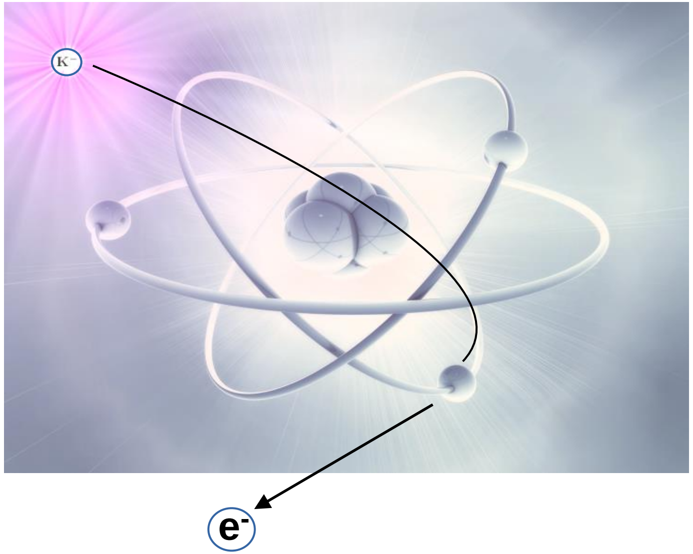

IN-FLIGHT

($p_K \sim 100$ MeV/c)

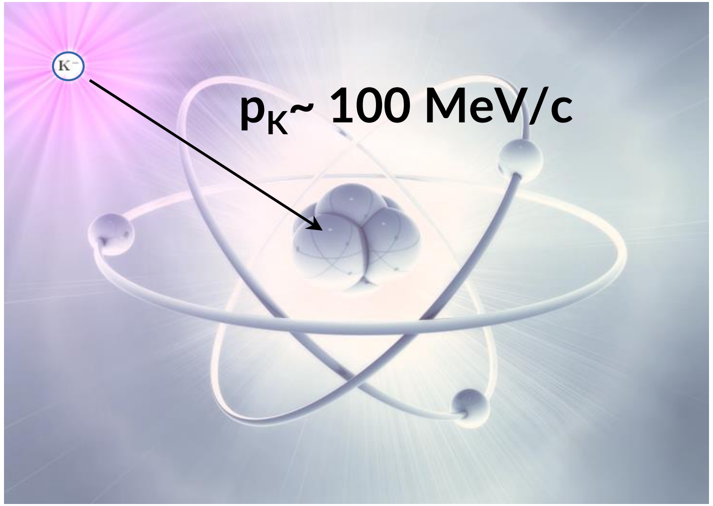

$K^- n \rightarrow \Lambda\pi^-$ events selection and interpretation

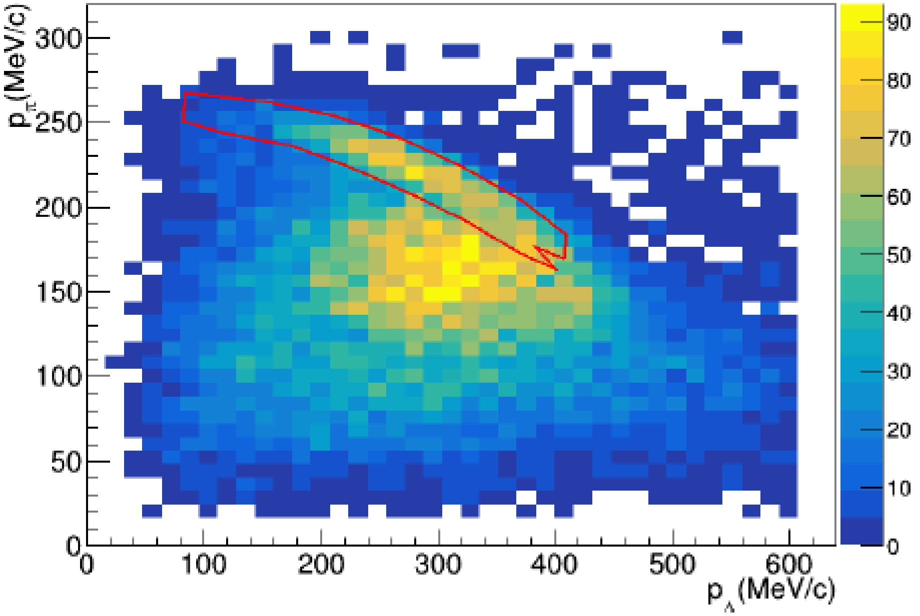

FIG. 2. *(Color online) Experimental distribution of the π^- vs Λ momenta. The red line represents the selection of the direct $\Lambda\pi^-$ production events. See the text for details.*

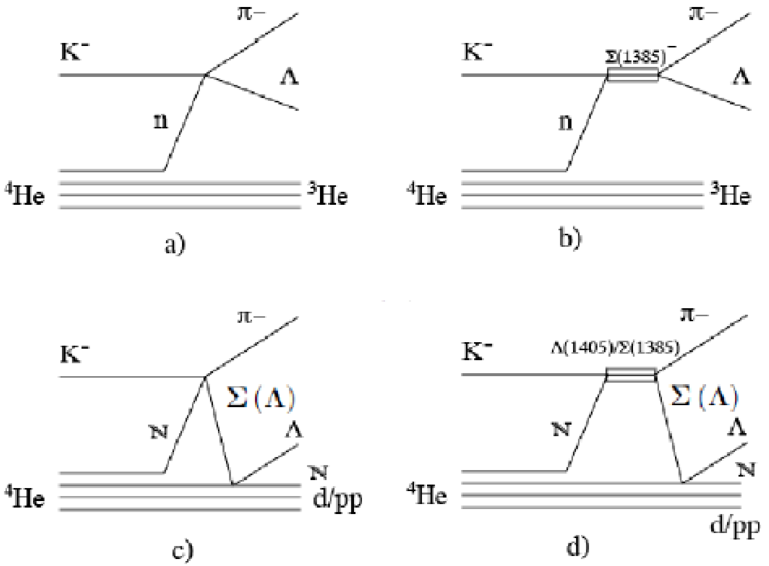

FIG. 1. *Panels a) and b) show the non-resonant and resonant $\Lambda\pi^-$ direct productions, respectively. Panels c) and d) show the primary hyperon-pion formation, followed by the inelastic/elastic scattering of the Σ/Λ hyperon on a single nucleon, for the resonant and non-resonant cases, respectively.*

Events selection - $\Lambda \rightarrow p\,\pi^-$ (BR = 63.9 ± 0.5%)

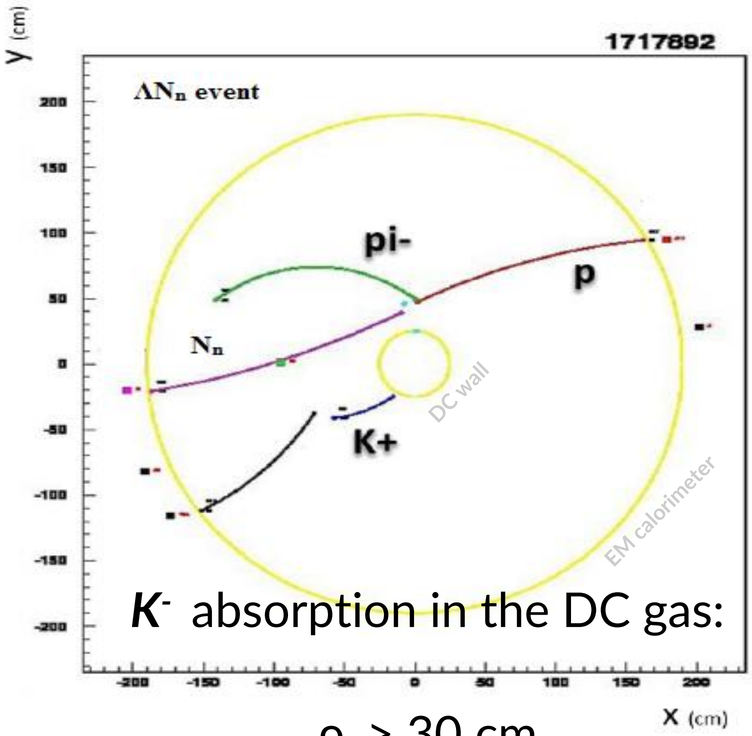

K^- absorption in the DC gas:

$\rho_\Lambda > 30$ cm

contamination with K^- absorption in the DC wall < 3%

Opposite charged tracks with common vertex,

main background: $(K^\pm \rightarrow \pi^\pm \pi^\pm \pi^\mp)$

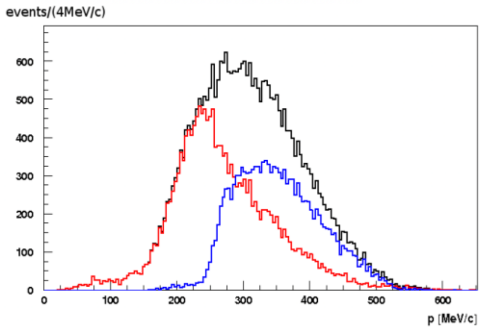

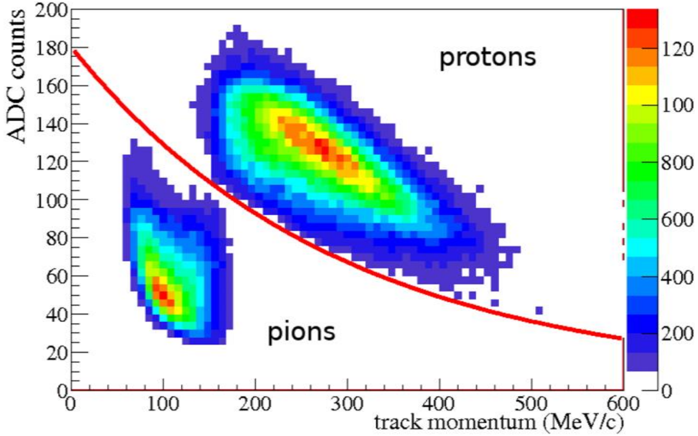

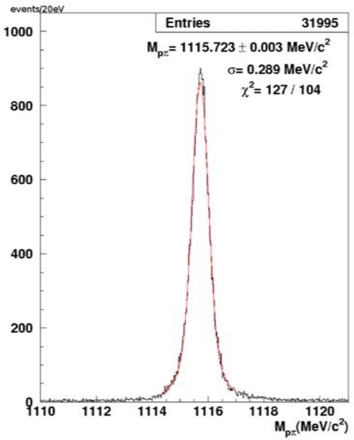

Simultaneous fit : $p_{\Lambda\pi^-}$ - $m_{\Lambda\pi^-}$ - $\cos\theta_{\Lambda\pi^-}$

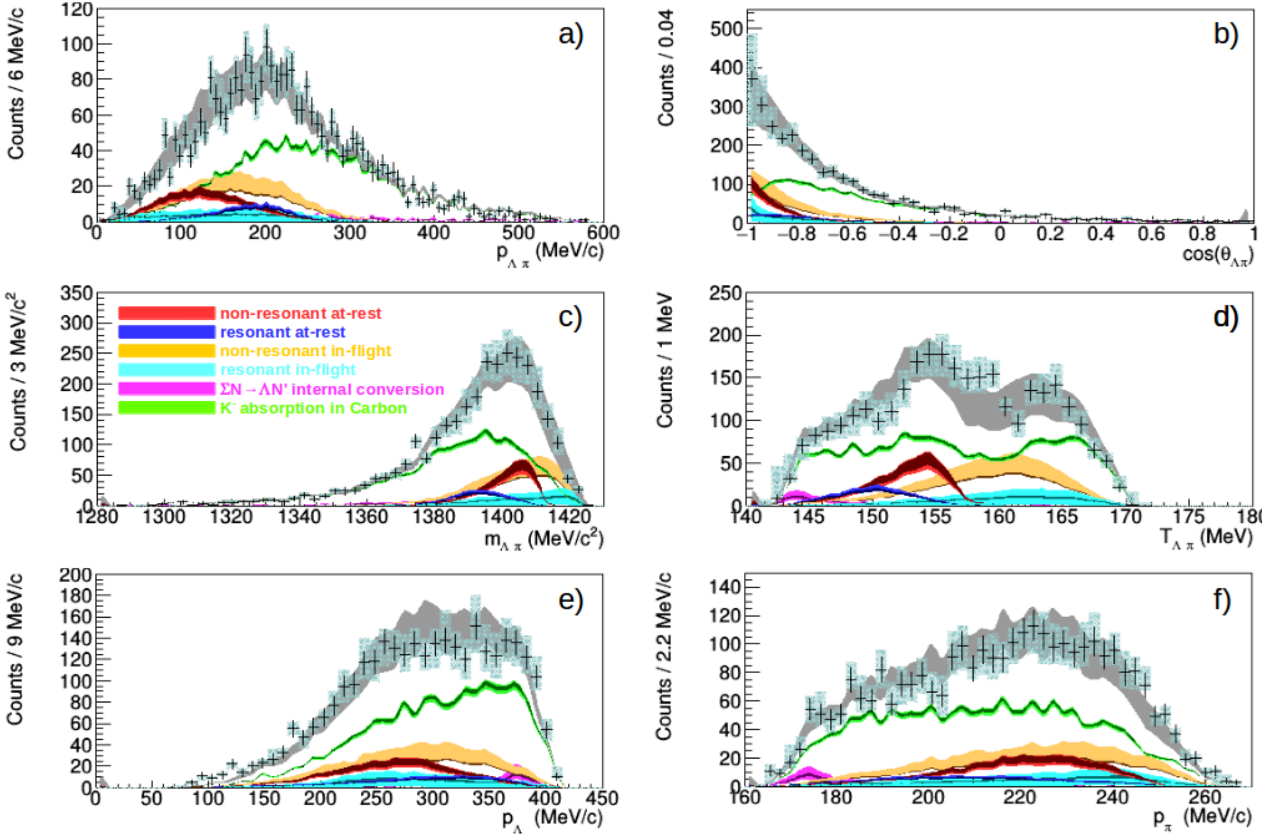

Investigated using:

K^- "n" $^3He \rightarrow \Lambda\pi^-\ ^3He$

$$E_{Kn} \sim -B_n - < \frac{p^2_{\Lambda\pi}}{2\mu_{\pi,\Lambda,3He}} >$$

33 ± 6 MeV below threshold

see also

A. Cieply et al., Phys. Lett. B 702 (2011) 402

T. Hoshino et al., Phys. Rev. C 96 (2017) 045204

N. Barnea, E. Friedman, A. Gal, Nucl. Phys. A968 (2017)

[K. P., S. Wycech, L. Fabbietti et al. Phys.Lett. B782 (2018) 339-345]

[K. P., S. Wycech, C. Curceanu, Nucl. Phys. A 954 (2016) 75-93]

Outcome of the measurement

Investigated using:

K^- **"n"** $^3He \rightarrow \Lambda\pi^- \; ^3He$

Energy of the K^-n system:

$$E_{\mathrm{Kn}} \sim -B_n - < \frac{p^2_{\Lambda\pi}}{2\mu_{\pi,\Lambda,3\mathrm{He}}} >$$

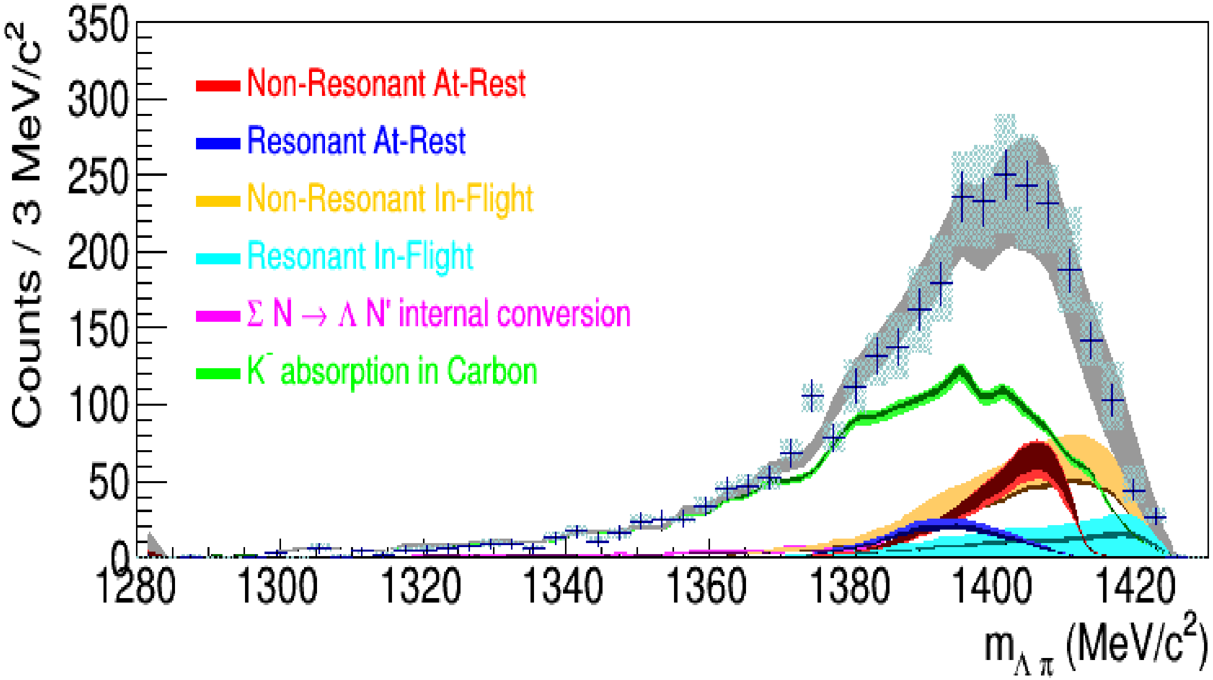

[K. P., S. Wycech, L. Fabbietti et al. Phys.Lett. B782 (2018) 339-345]
[K. P., S. Wycech, C. Curceanu, Nucl. Phys. A 954 (2016) 75-93]

Outcome of the measurement

Investigated using: **K$^-$ "n"** ^{3}He → **Λπ$^-$** ^{3}He

$$|f_{ar}^{nr}| = (0.334 \pm 0.018\,\text{stat}^{+0.034}_{-0.058}\text{syst})\ \text{fm}$$

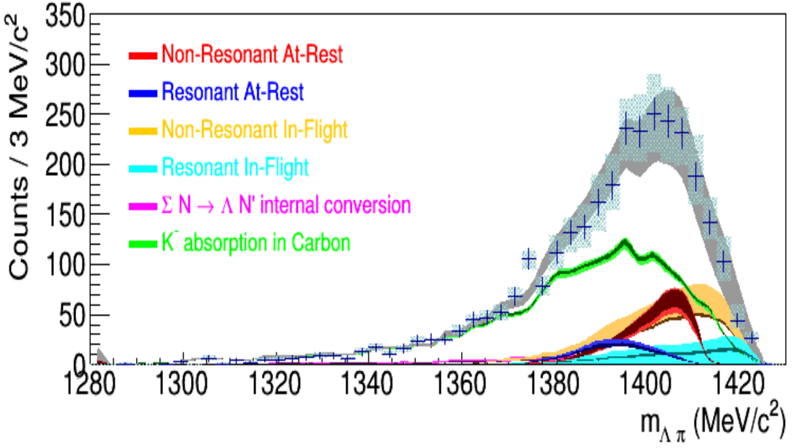

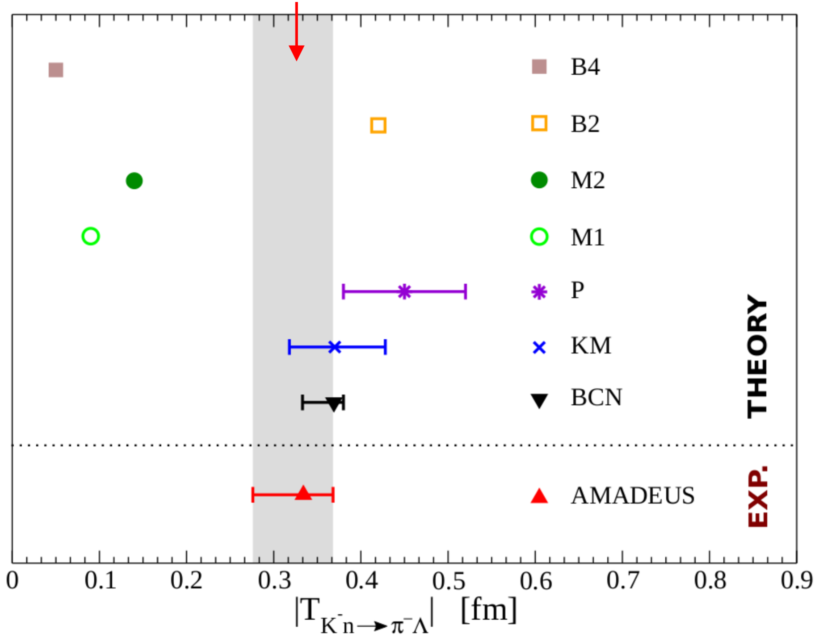

[K. P., S. Wycech, L. Fabbietti et al. Phys.Lett. B782 (2018) 339-345]
[K. P., S. Wycech, C. Curceanu, Nucl. Phys. A 954 (2016) 75-93]

Simultaneous/independent measurement of the

$K^- p \rightarrow \Sigma^0 \pi^0$ & $\Lambda \pi^0$

cross sections at $p_{K^-} = 98 \pm 10$ MeV/c

Events selection - γ_1, γ_2 & γ_3

$$K^- \text{"}p\text{"} \rightarrow \Sigma^0 \pi^0 \rightarrow (\Lambda \gamma_3)(\gamma_1 \gamma_2) \rightarrow (p\pi^-)\gamma_1\gamma_2\gamma_3$$

- $K^+ \rightarrow \pi^+\pi^0$ background is rejected
- three photon clusters are selected by TOF

$$\chi_t^2 = t^T V_t^{-1} t$$

with $t = t_i - t_j$; $t_i = t_{cli} - r_i/c$

- disentangling γ_1, γ_2 & γ_3 :

$$\chi^2_{\pi\Sigma} = \frac{(m_{\pi^0} - m_{ij})^2}{\sigma^2_{ij}} + \frac{(m_{\Sigma^0} - m_{k\Lambda})^2}{\sigma^2_{k\Lambda}}$$

- MC based rejection criteria:

$$\chi_t^2 \leq 20,\ \chi^2_{m_{\gamma_1\gamma_2}} \leq 5 \text{ and } \chi^2_{m_{\Lambda\gamma_3}} \leq 4$$

- Cluster splitting background free! Algorithm overall efficiency for γ detection: 0.98 ± 0.01.

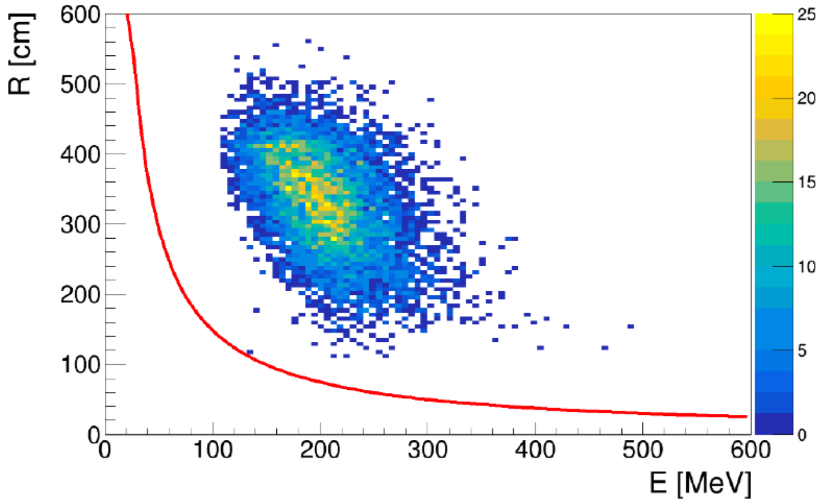

Events selection - Σ^0 & π^0

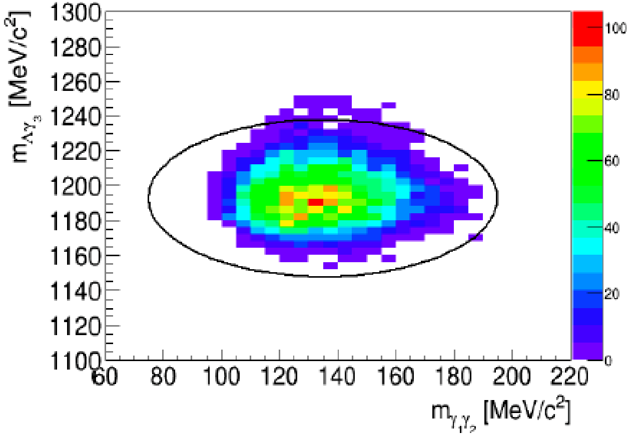

FIG. 1. The plot shows the $m_{\Lambda\gamma_3}$ distribution as a function of $m_{\gamma_1\gamma_2}$. A black ellipse represents the applied selection in the two invariant masses space.

$$\frac{\left(m_{\Lambda\gamma_3} - m_{\Sigma^0}\right)^2}{(3\sigma_{\Lambda\gamma_3})^2} + \frac{\left(m_{\gamma_1\gamma_2} - m_{\pi^0}\right)^2}{(3\sigma_{\gamma_1\gamma_2})^2} < 1$$

- RESOLUTIONS:

$\sigma_{\Lambda\gamma_3}$ ~15 MeV/c and $\sigma_{\gamma_1\gamma_2}$ ~20 MeV/c

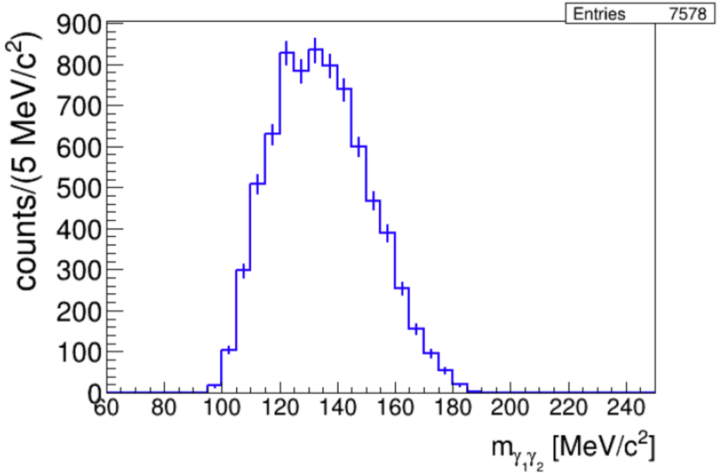

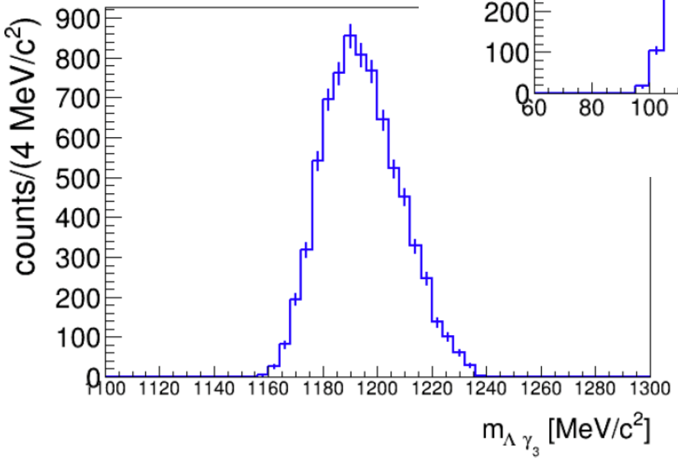

Events selection - K^- H abs. in flight

- **SIGNAL**: K^- H -> $(\Sigma^0 / \Lambda)\ \pi^0$ (*if*)

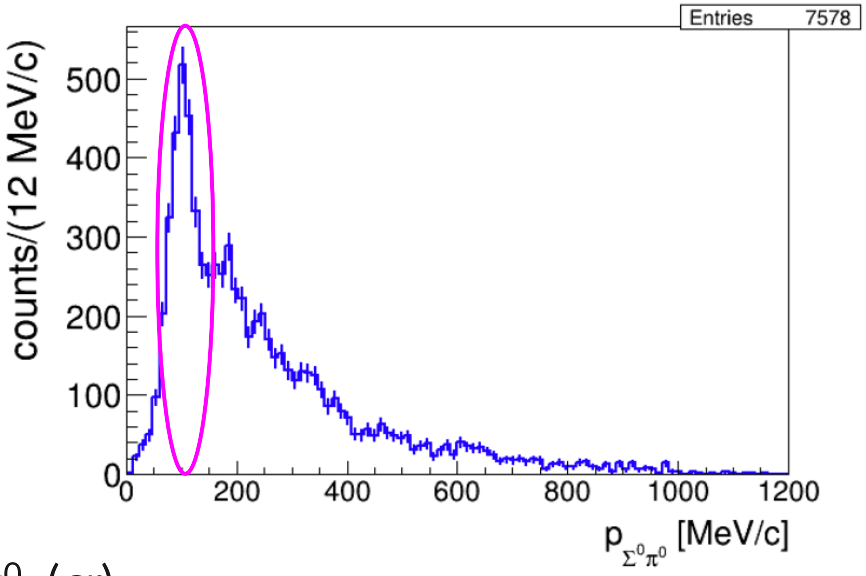

- **BACKGROUND**: K^- H -> $(\Sigma^0 / \Lambda)\ \pi^0$ (*ar*)
  K^- $(^4He/^{12}C)$ -> $(\Sigma^0 / \Lambda)\ \pi^0$ + Residual (*ar* + *if*)
  elastic or inelastic FSI of the hyperon (Y) and/or the π^0

- **FURTHERMORE** in $\Lambda\pi^0$ the direct production is affected by the background: $\Sigma^0\pi^0$ primary production followed by $\Sigma^0 \to \Lambda\gamma$ for ALL the channels

Events selection - K^- H abs. in flight

- **SIGNAL**: K^- H -> $(\Sigma^0 / \Lambda)\ \pi^0$ (*if*)

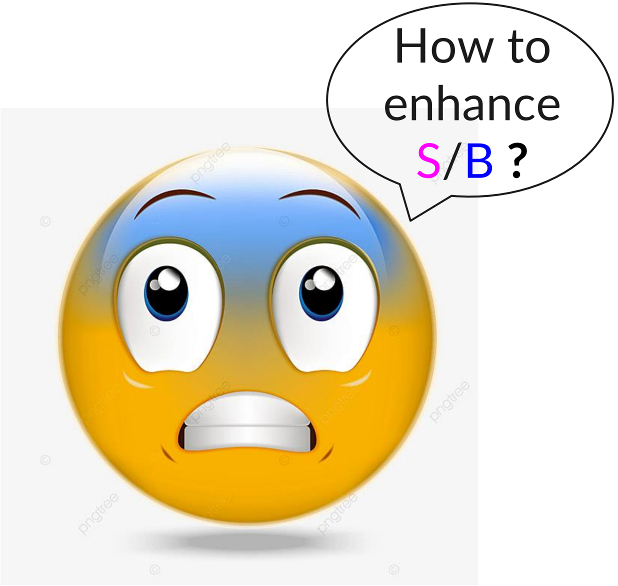

- **BACKGROUND**: K^- H -> $(\Sigma^0 / \Lambda)\ \pi^0$ (*ar*)
  K^- ($^4He/^{12}C$) -> $(\Sigma^0 / \Lambda)\ \pi^0$ + Residual (*ar + if*)
  elastic or inelastic FSI of the hyperon (Y) and/or the π^0

- **FURTHERMORE** in $\Lambda \pi^0$ the direct production is affected by the background: $\Sigma^0 \pi^0$ primary production followed by $\Sigma^0 \to \Lambda\gamma$ for ALL the channels

Events selection - K^- H abs. in flight

SIGNAL: K^- H -> (Σ^0 / Λ) π^0 *(if)*
characteristic features:

a) the kinematics (for both ar & if)
is completely determined by E-p cons.
signal is almost back to back,

b) K^- H -> Λ π^0 *(ar & if)* events can be
sampled exploiting the resolution on p_Λ

$\sigma_{p\Lambda}$= 1.9 ± 0.2 MeV/c

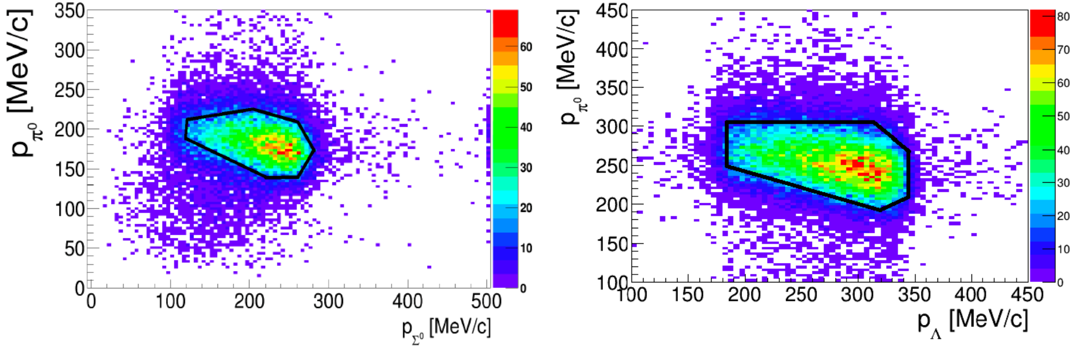

FIG. 2. The plot shows reconstructed MC p_{π^0} vs. p_Y distributions for the K^- H $\to \Sigma^0 \pi^0$ *if* reaction (top) and K^- H $\to \Lambda \pi^0$ *if* reaction (bottom). The phase space selections are represented as black contours.

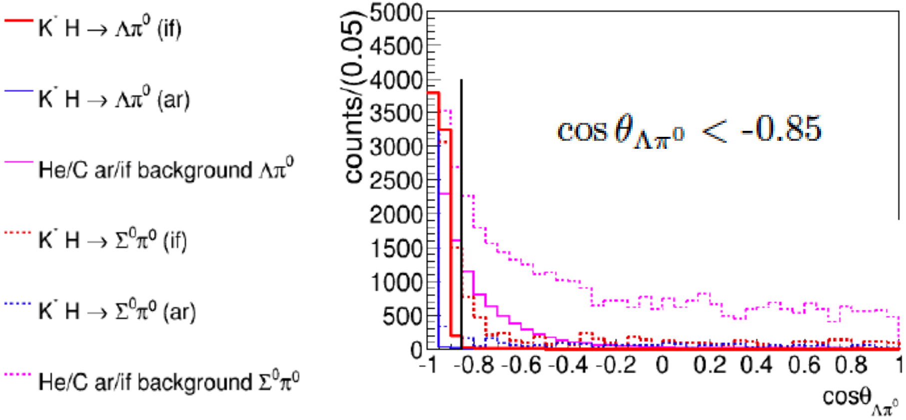

Events selection - K^- H abs. in flight

c) due to E-p cons. the total $Y\pi^0$ momentum distribution for K^- H -> Y π^0 (*if*) events reflects the original K^- momentum spectrum

FSI is negligible after phase-space selections, is considered in systematics.

residual bkg: K^- H (*ar*) and K^- (^{4}He/^{12}C)
can be efficiently disentangled by means of a simultaneous fit

arbitrary normalization

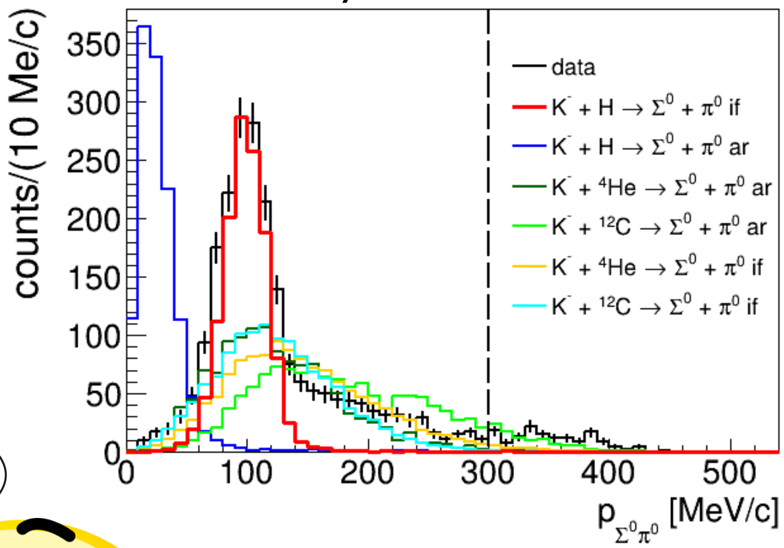

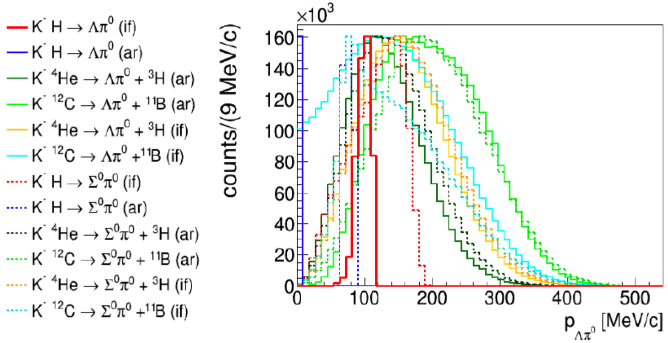

Simultaneous fit and cross sections ($\Sigma^0\pi^0$)

$$\chi^2 = \sum_q \sum_{n=1}^{N^q_{bins}} \frac{(N^q_n - \mathcal{F}^q(q_n))^2}{\sigma^{q2}_n} \quad \text{with} \quad \mathcal{F}^q(q_n) = \sum_{i=1}^{N_{par}} \alpha_i \cdot h^q_i(q_n)$$

physical processes:

1. $K^- H \rightarrow (\Sigma^0/\Lambda)\,\pi^0\ if$ (red),
2. $K^- H \rightarrow (\Sigma^0/\Lambda)\,\pi^0\ ar$ (blue),
3. $K^- + {}^4He/{}^{12}C \rightarrow \Sigma^0/\Lambda + \pi^0 + {}^3H/{}^{11}B$ (magenta).

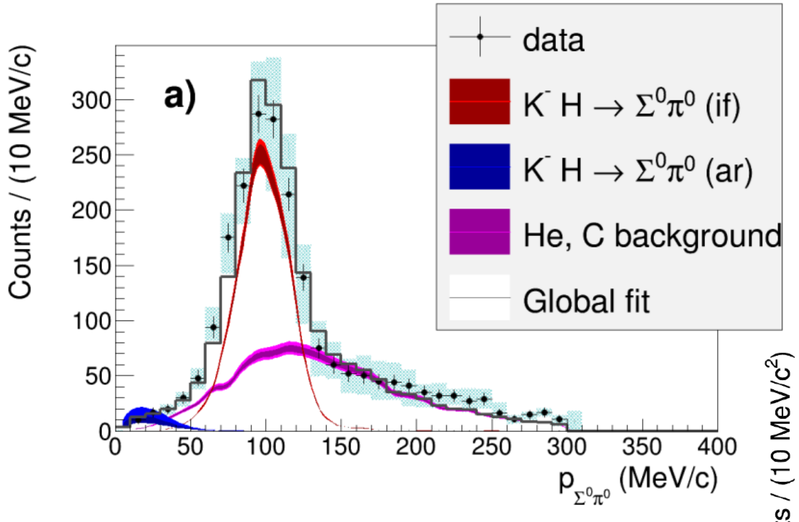

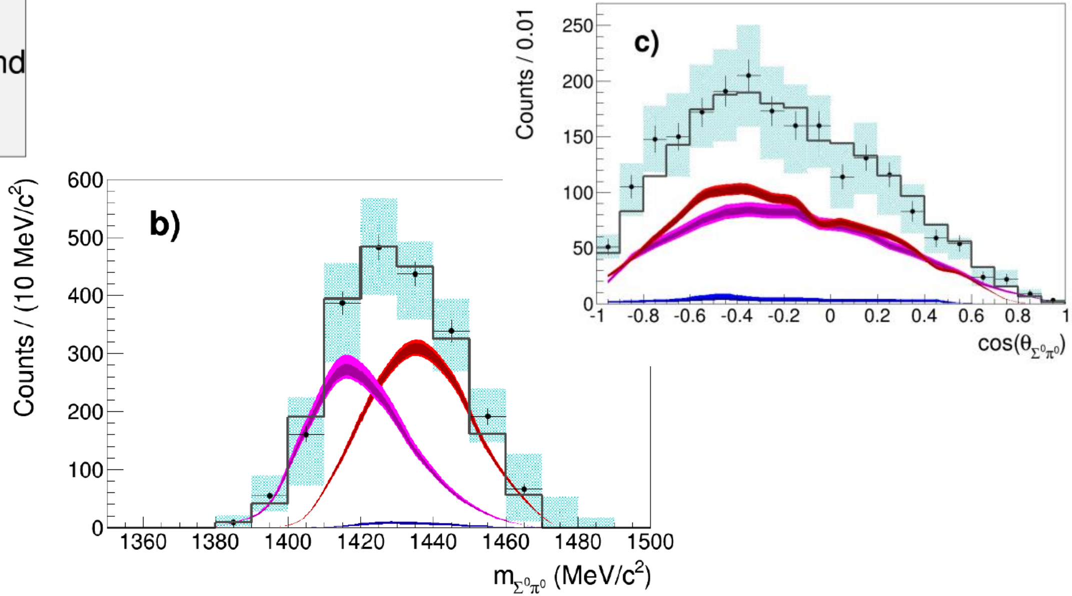

FIG. 3. From top to bottom the figure shows the result of the simultaneous fit of $p_{\Sigma^0\pi^0}$, $m_{\Sigma^0\pi^0}$ and $cos\theta_{\Sigma^0\pi^0}$. The experimental data and the corresponding statistical errors are represented by black crosses, the systematic errors are light blue boxes. The contributions of the various physical processes are shown as colored histograms, according to the color code shown in the caption. The light and dark bands correspond to systematic and statistical errors, respectively. The gray distribution reproduces the global fit function.

Simultaneous fit and cross sections ($\Lambda\,\pi^0$)

physical processes:

1. $K^- H \quad \rightarrow \quad (\Sigma^0/\Lambda)\,\pi^0\ if$ (red),
2. $K^- H \quad \rightarrow \quad (\Sigma^0/\Lambda)\,\pi^0\ ar$ (blue),
3. $K^- + {}^4He/{}^{12}C \quad \rightarrow \quad \Sigma^0/\Lambda + \pi^0 + {}^3H/{}^{11}B$ (magenta).

\+ the same processes initiated by primary $\Sigma^0\,\pi^0$ and followed by $\Sigma^0 \to \Lambda\gamma$

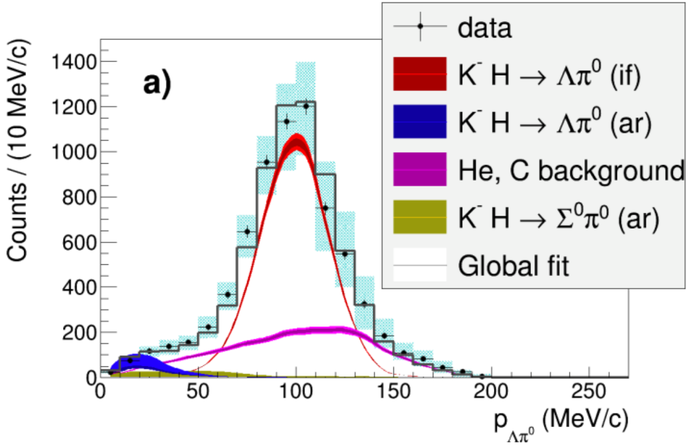

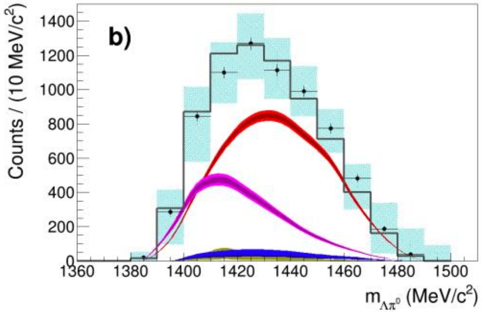

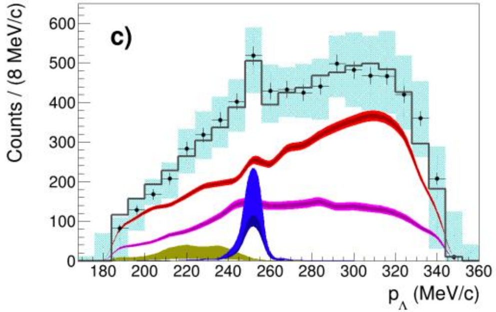

FIG. 4. From top to bottom the figure shows the result of the simultaneous fit of $p_{\Lambda\pi^0}$, $m_{\Lambda\pi^0}$, p_Λ and p_{π^0}. The experimental data and the corresponding statistical errors are represented by black crosses, the systematic errors are light blue boxes. The contributions of the various physical processes are shown as colored histograms, according to the color code shown in the caption. The light and dark bands correspond to systematic and statistical errors, respectively. The gray distribution reproduces the global fit function.

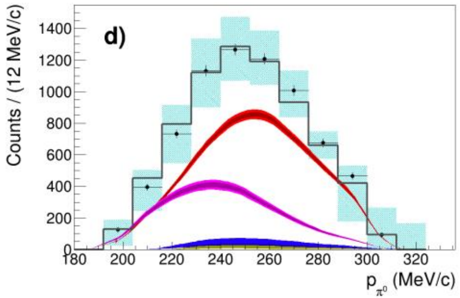

Cross sections results

1 o.m. improvement on the relative error

$\Sigma^0 - \pi^0$ CHANNEL $\frac{\chi^2}{(dof-np)} = \frac{92}{54} = 1.71$		
process	fit par. value	$\sigma_{stat.}$
$K^- H \to \Sigma^0 \pi^0 \,(if)$	0.511	$\pm$ 0.018
$K^- H \to \Sigma^0 \pi^0 \,(ar)$	0.017	$\pm$ 0.005
$K^- +^4 He/^{12}C \to \Sigma^0 \pi^0$		
+ residual (ar/if)	0.463	$\pm$ 0.018
$\Lambda - \pi^0$ CHANNEL $\frac{\chi^2}{(dof-np)} = \frac{165}{57} = 2.95$		
process	fit par. value	$\sigma_{stat.}$
$K^- H \to \Lambda \pi^0 \,(if)$	0.659	$\pm$ 0.011
$K^- H \to \Lambda \pi^0 \,(ar)$	0.021	$\pm$ 0.003
$K^- +^4 He/^{12}C \to \Lambda \pi^0$		
+ residual (ar/if)	0.298	$\pm$ 0.012
$K^- H \to \Sigma^0 \pi^0$		
$\to \Lambda \gamma \pi^0 \,(ar)$	0.018	$\pm$ 0.006

TABLE I. The table summarizes the results obtained from the fits of the $\Sigma^0\pi^0$ and $\Lambda\pi^0$ samples. The values of the reduced chi-squares and of the fit parameters are summarized.

cross section at p_{K^-} = 98 ± 10 MeV/c :

- $\sigma_{K^-p\to\Sigma^0\pi^0} = 42.8 \pm 1.5(stat.)^{+2.4}_{-2.0}(syst.)\ \mathrm{mb}$
- $\sigma_{K^-p\to\Lambda\pi^0} = 31.0 \pm 0.5(stat.)^{+1.2}_{-1.2}(syst.)\ \mathrm{mb}$,

arXiv:2210.10342 [nucl-ex]
Accepted PRC

Λp analysis: $K^- + {}^{12}C \rightarrow \Lambda + p + R$

Simultaneous fit of:

- Λp invariant mass;
- angular correlation;
- proton momentum;
- Λ momentum.

Total reduced χ^2: χ^2/dof = 0.94

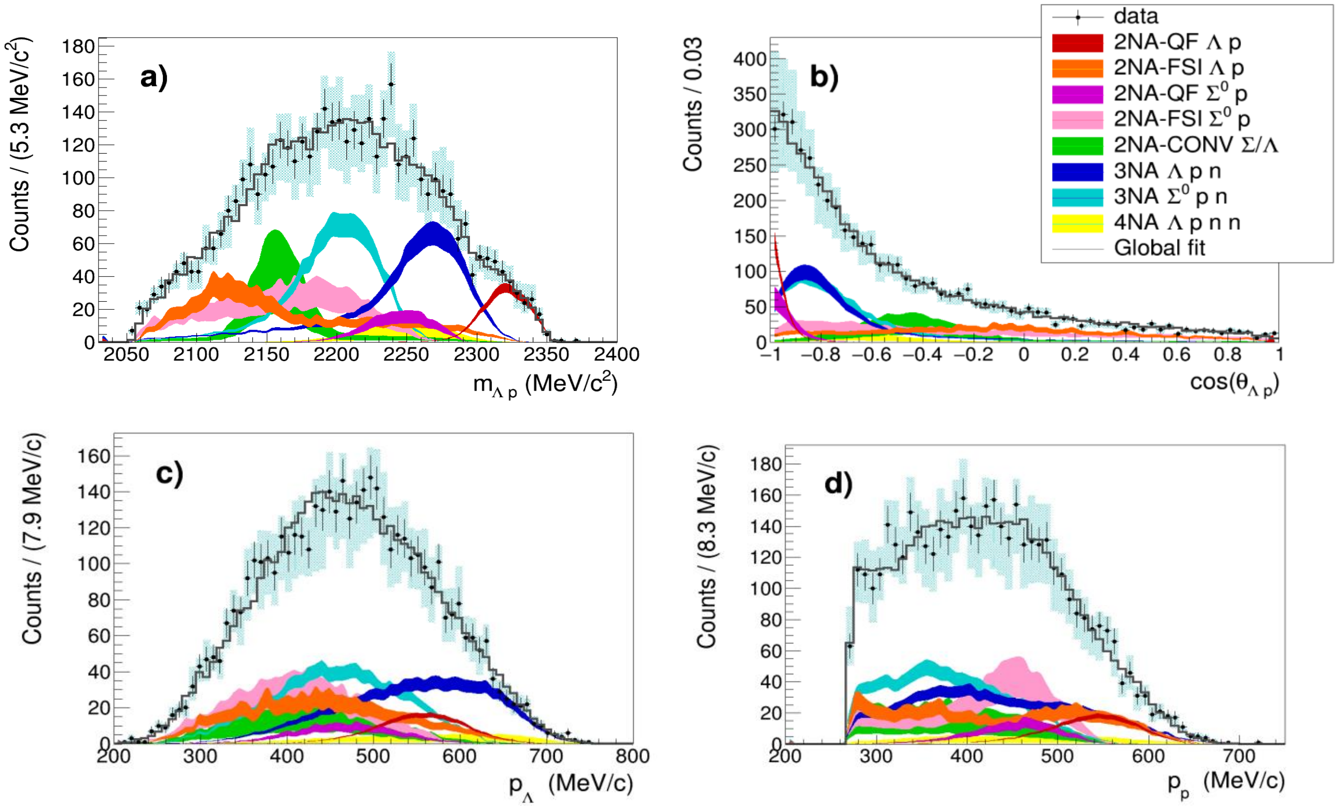

[R. Del Grande, K. P., O. Vazquez Doce et al., Eur.Phys.J. C79 (2019) no.3, 190]
[R. Del Grande, K. P., S. Wycech, Acta Phys. Pol. B 48 (2017) 1881]
[O. Vazquez Doce, L. Fabbietti et al., Phys.Lett. B 758, 134-139 (2016)]

Λp analysis: K⁻ multi-nucleon absorption BRs and σ

[R. Del Grande, K. P., O. Vazquez Doce et al., Eur.Phys.J. C79 (2019) no.3, 190]

Process	Branching Ratio (%)	σ (mb)	@	p_K (MeV/c)
2NA-QF Λp	0.25 ± 0.02 (stat.) $^{+0.01}_{-0.02}$(syst.)	2.8 ± 0.3 (stat.) $^{+0.1}_{-0.2}$ (syst.)	@	128 ± 29
2NA-FSI Λp	6.2 ± 1.4(stat.) $^{+0.5}_{-0.6}$(syst.)	69 ± 15 (stat.) $\pm$ 6 (syst.)	@	128 ± 29
2NA-QF Σ^0p	0.35 ± 0.09(stat.) $^{+0.13}_{-0.06}$(syst.)	3.9 ± 1.0 (stat.) $^{+1.4}_{-0.7}$ (syst.)	@	128 ± 29
2NA-FSI Σ^0p	7.2 ± 2.2(stat.) $^{+4.2}_{-5.4}$(syst.)	80 ± 25 (stat.) $^{+46}_{-60}$ (syst.)	@	128 ± 29
2NA-CONV Σ/Λ	2.1 ± 1.2(stat.) $^{+0.9}_{-0.5}$(syst.)	-		
3NA Λpn	1.4 ± 0.2(stat.) $^{+0.1}_{-0.2}$(syst.)	15 ± 2 (stat.) $\pm$ 2 (syst.)	@	117 ± 23
3NA Σ^0pn	3.7 ± 0.4(stat.) $^{+0.2}_{-0.4}$(syst.)	41 ± 4 (stat.) $^{+2}_{-5}$ (syst.)	@	117 ± 23
4NA Λpnn	0.13 ± 0.09(stat.) $^{+0.08}_{-0.07}$(syst.)	-		
Global $\Lambda(\Sigma^0)$p	21 ± 3(stat.) $^{+5}_{-6}$(syst.)	-		

The ratio between the branching ratios of the 2NA-QF in the Λp channel and in the Σ^0p is measured to be:

$$\mathcal{R} = \frac{BR(K^- pp \rightarrow \Lambda p)}{BR(K^- pp \rightarrow \Sigma^0 p)} = 0.7 \pm 0.2(stat.)^{+0.2}_{-0.3}(syst.)$$

and the ratio between the corresponding phase spaces is $\mathcal{R}' \simeq 1.22$.

Information on the in-medium dynamics

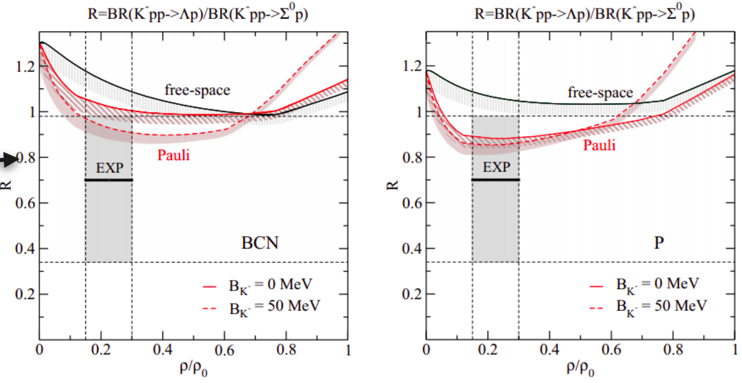

[J. Hrtánková and A. Ramos. Phys. Rev. C, 101(3):035204, 2020]

Total BR of the K^- 2NA process in ^{12}C

the only missing components are:

- BR(Σ^-n) = (0.12 ± 0.01(syst.))%
- BR(QF-Λn + QF-Σ^0n) = $(0.76 \pm 0.09(\text{stat.})\,^{+0.13}_{-0.06}\,(\text{syst.}))\%$
- BR(FSI-Λn + FSI-Σ^0n) = $(1.62 \pm 0.04(\text{stat.})\,^{+0.22}_{-0.21}\,(\text{syst.}))\%$
- BR(no conv Σ^+ and Σ^-) = (3.04 ± 0.03(stat.) ± 0.92(syst.))%

→ $(5.5 \pm 0.1(\text{stat.})\,^{+1.0}_{-0.9}\,(\text{syst.}))\%$

[R. Del Grande, K. P., et al., 2020 Phys. Scr.95 084012]
[R. Del Grande, K. P., et al., *Few Body Syst.* 62 (2021) 1, 7]

Including the missing components the total BR of the K^-2NA is:

$$\mathrm{BR}(\mathrm{K}^-2\mathrm{NA} \rightarrow \mathrm{YN}) = (21.6 \pm 2.9(\mathrm{stat.})^{+4.4}_{-5.6}(\mathrm{syst.}))\%$$

to be compared with [J. Hrtánková and A. Ramos. Phys. Rev. C, 101(3):035204, 2020]

Λp analysis: K⁻ pp bound state

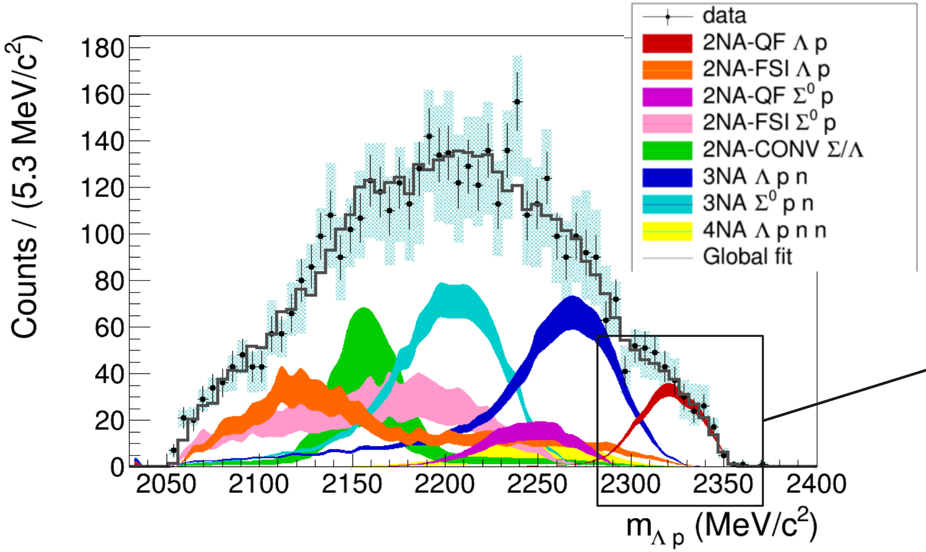

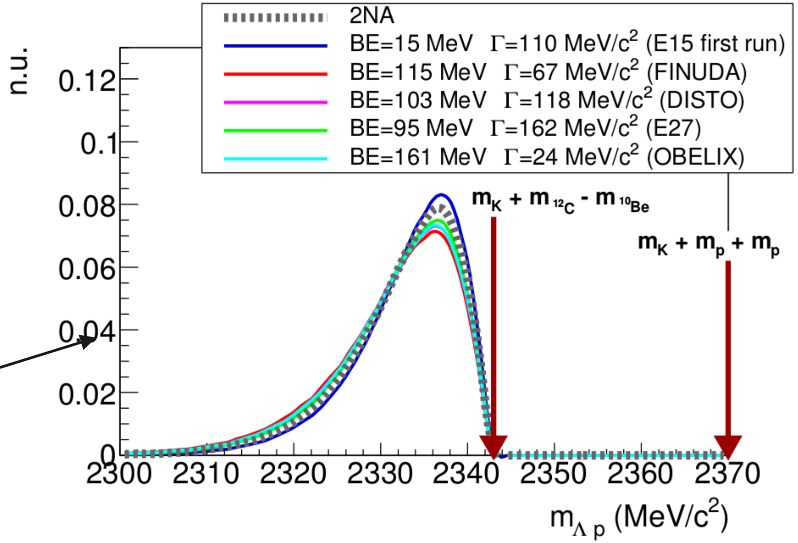

K^-pp bound state contribution **completely overlaps** with the K^-2NA

Λp analysis: K^- pp bound state

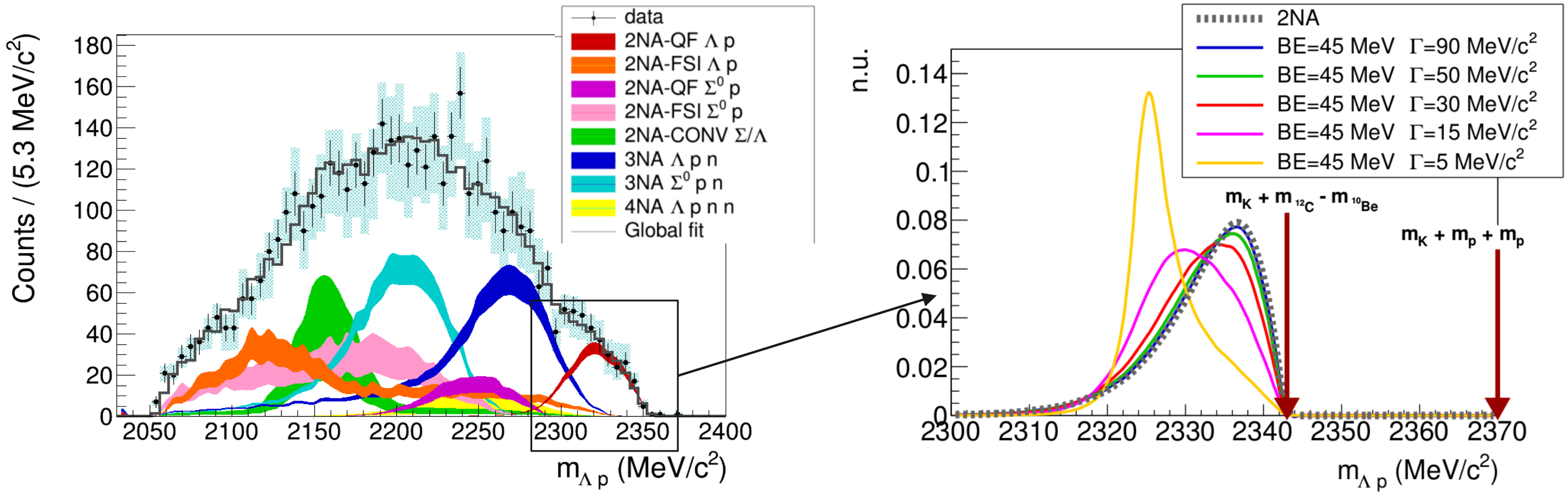

K^-pp bound state contribution **completely overlaps** with the K^-2NA

Λp analysis: K^- pp bound state search

AMADEUS at DAΦNE

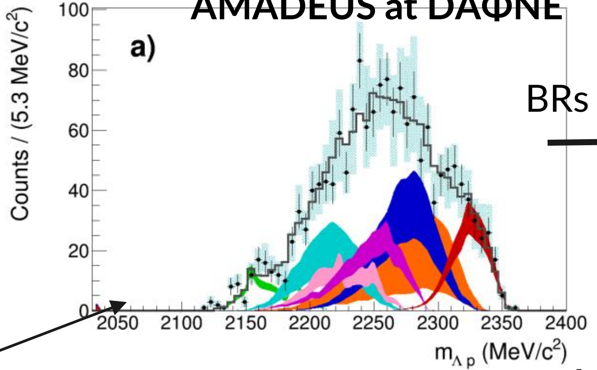

BRs evaluation

Process	Branching Ratio (%)
2NA-QF Λp	$0.20 \pm 0.04(\text{stat.}) \pm 0.02(\text{syst.})$
2NA-FSI Λp	$3.8 \pm 2.3(\text{stat.}) \pm 1.1(\text{syst.})$
2NA-QF Σ^0p	$0.54 \pm 0.20(\text{stat.}) ^{+0.20}_{-0.16}(\text{syst.})$
2NA-FSI Σ^0p	$5.4 \pm 1.5(\text{stat.}) ^{+1.0}_{-2.7}(\text{syst.})$
2NA-CONV Σ/Λ	$22 \pm 4(\text{stat.}) ^{+1}_{-12}(\text{syst.})$
3NA Λpn	$1.1 \pm 0.3(\text{stat.}) \pm 0.2(\text{syst.})$
3NA Σ^0pn	$1.9 \pm 0.7(\text{stat.}) ^{+0.8}_{-0.4}(\text{syst.})$

only **back-to-back** Λp pairs ($\cos\theta_{\Lambda p} < -0.8$)

FINUDA at DAΦNE

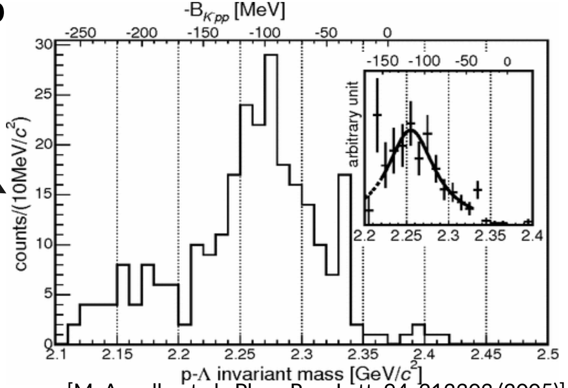

[M. Agnello et al., Phys. Rev. Lett. 94, 212303 (2005)]

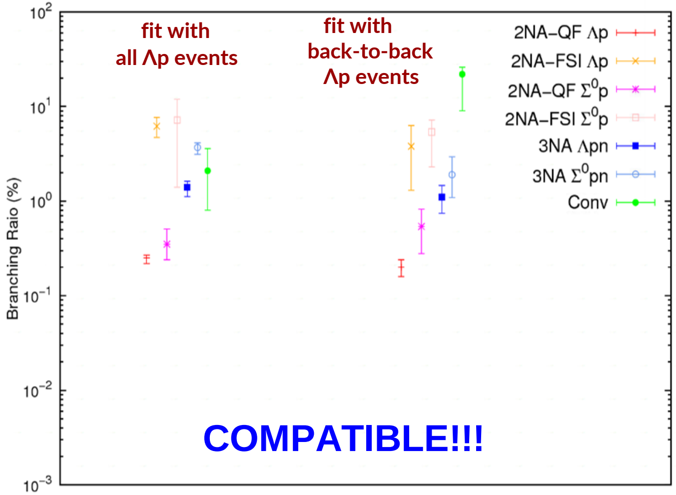

In agreement with

V.K. Magas, E. Oset, A. Ramos, H. Toki,. Phys. Rev. C 74, 025206 (2006)
V.K. Magas, E. Oset, A. Ramos,. Phys. Rev. C 77, 065210 (2008)

Λt analysis: Cross section and BR for 4NA

GOLDEN CHANNEL to extrapolate the K^- 4NA

K^- + "ppnn" → Λ + t

Previous data:

- in ^{4}**He:** bubble chamber experiment

/M. Roosen, J. H. Wickens, Il Nuovo Cimento 66, 101 (1981)/

only **3 events** compatibile with Λt kinematics found

BR(K^- ^{4}He → Λt) = (3 ± 2) × 10^{-4} /K_{stop} → global, no 4NA

- in **solid targets:** ^{6,7}**Li,** ^{9}**Be** (FINUDA)

/Phys. Lett. B, 229 (2008)/

40 events, only **back-to-back data**

Λt emission yield → 10^{-3} – 10^{-4} / K^-_{stop}

→ global, no 4NA

PRELIMINARY

AMADEUS analysis

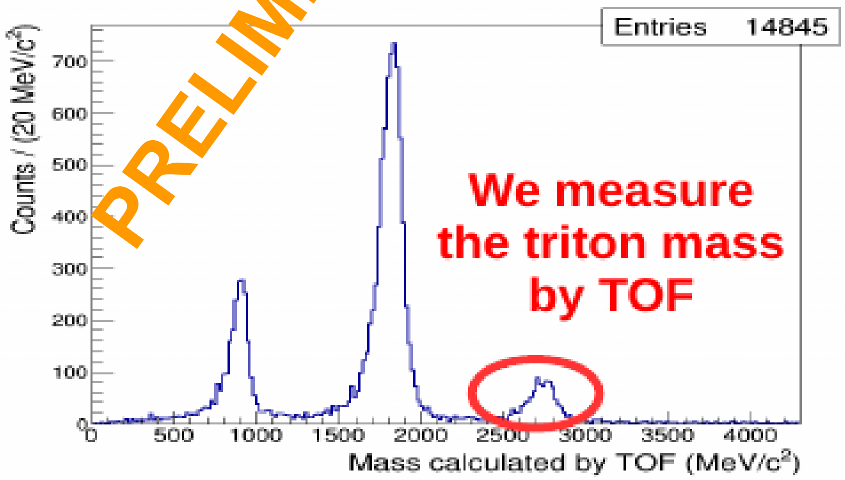

We measure the triton mass by TOF

MC simulations: efficiency & resolution

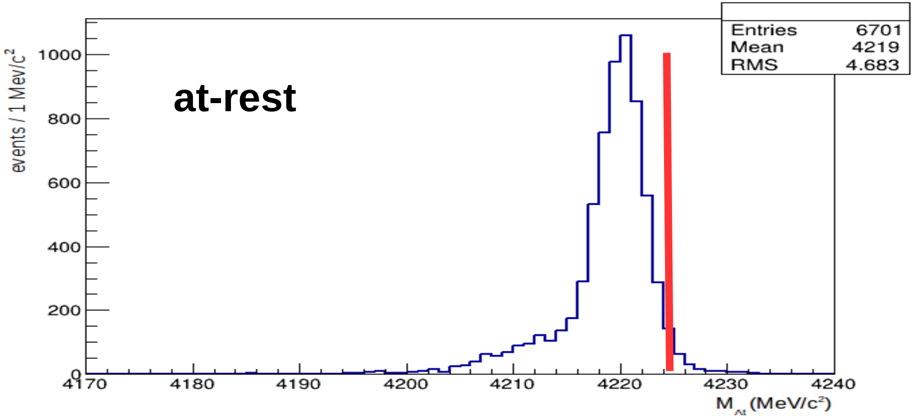

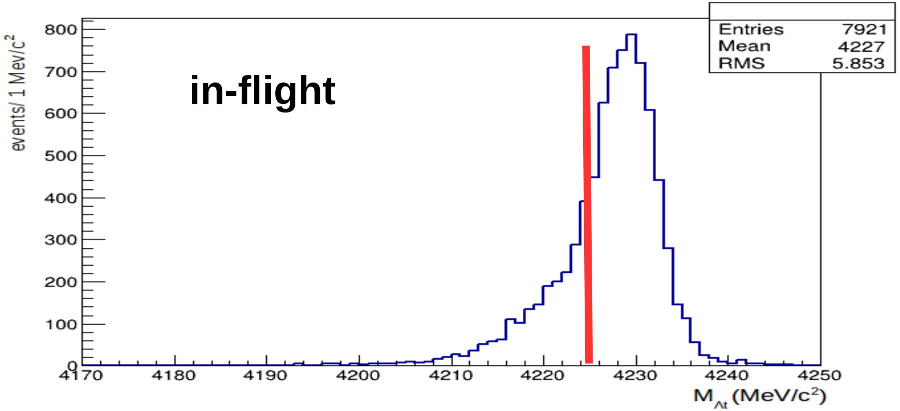

mass threshold at-rest

$M_{\Lambda t}$ invariant mass resolution = 2.2 MeV/c^2

overall <u>detection + reconstruction efficiency</u> for 4NA direct Λt production :

$$\epsilon_{4NA,ar,\Lambda t} = 0.0493 \pm 0.0006 \quad ; \quad \epsilon_{4NA,if,\Lambda t} = 0.0578 \pm 0.0006,$$

at-rest **in-flight**

Cross section and BR for 4NA in $K^{-}\,{}^{4}He \rightarrow \Lambda t$ process

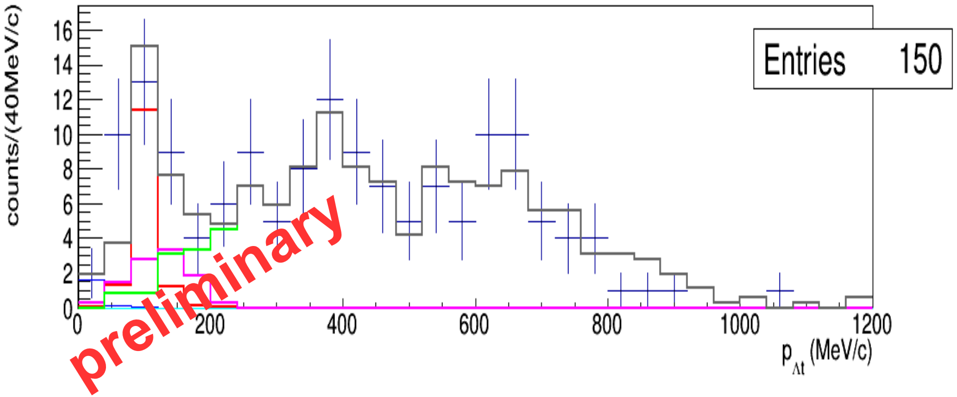

BR$(K^{-}\,{}^{4}He(4NA) \rightarrow \Lambda t)$ **< 2.0 × 10^{-4} /K_{stop} (95% c. l.)**

σ(100 ± 19 MeV/c) $(K^{-}\,{}^{4}He(4NA) \rightarrow \Lambda t)$ =
= **(0.81 ± 0.21 (stat) $^{+0.03}_{-0.04}$ (syst)) mb**

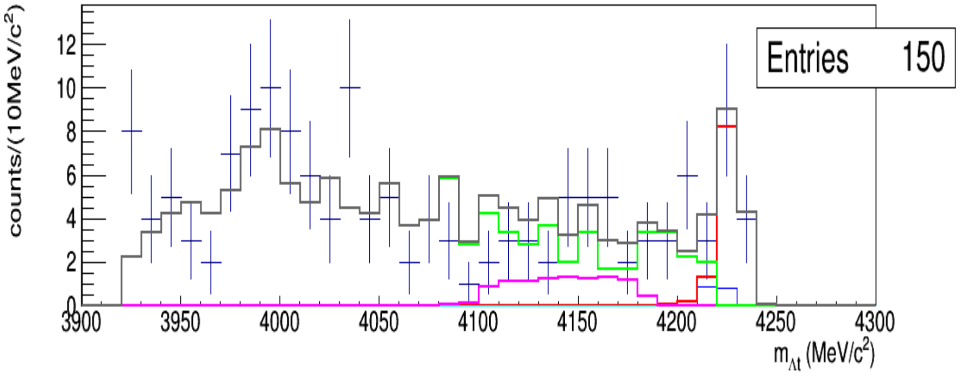

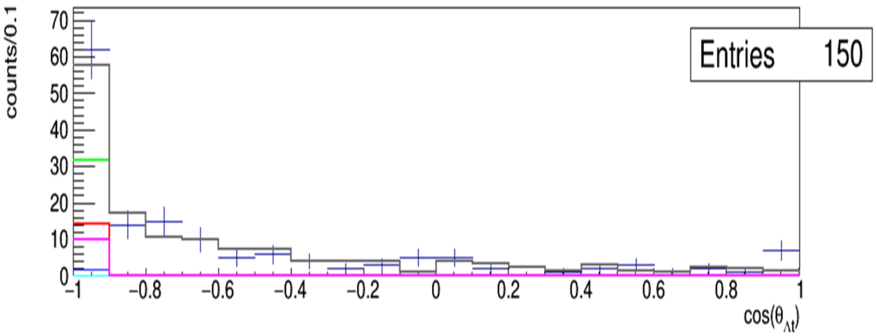

Cross section and BR for 4NA in $K^{-}\,{}^{12}C \rightarrow \Lambda/\Sigma^{0}\, t$ processes

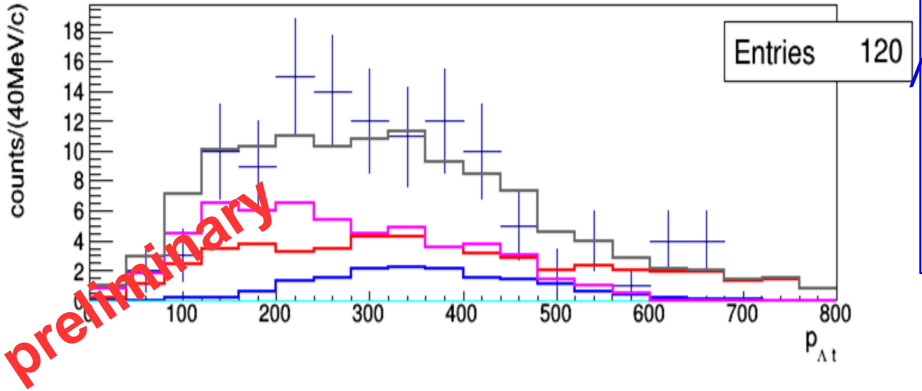

BR($K^{-12}C$(4NA) $\rightarrow \Lambda t\, {}^{8}Be$) = **$1.5 \pm 0.5 \times 10^{-4}$ (stat)** /K_{stop}

σ($K^{-12}C$ (4NA) $\rightarrow \Lambda t\, {}^{8}Be$) = **0.58 ± 0.11 (stat) mb**

σ($K^{-12}C$ (4NA) $\rightarrow \Sigma^{0} t\, {}^{8}Be$) = **1.88 ± 0.35 (stat) mb**

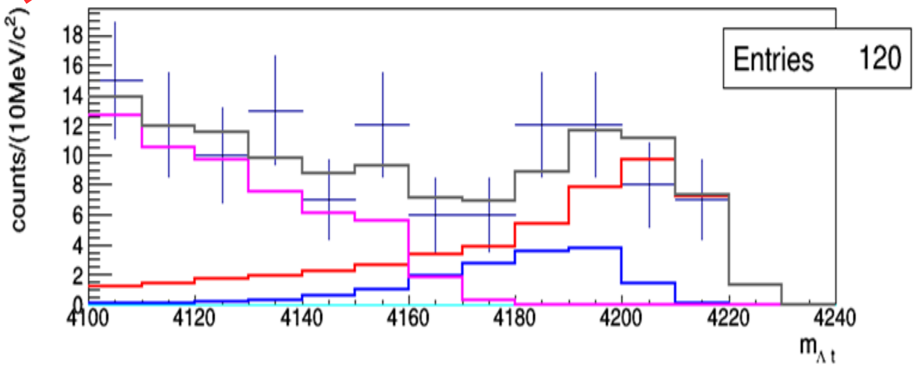

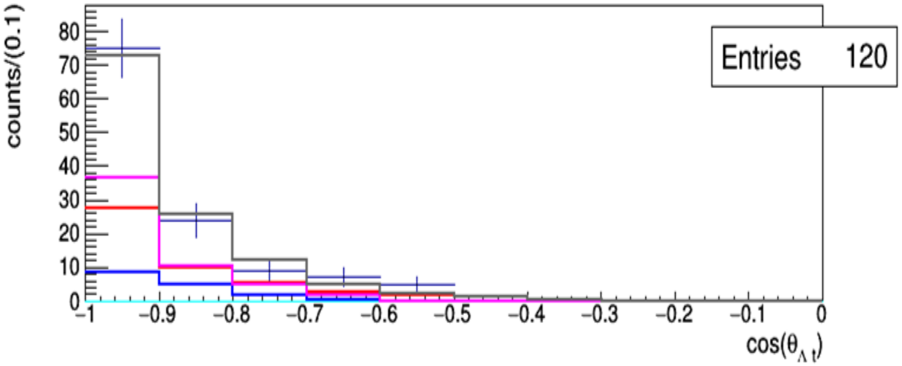

Highlights of AMADEUS results

K^-n amplitude below threshold

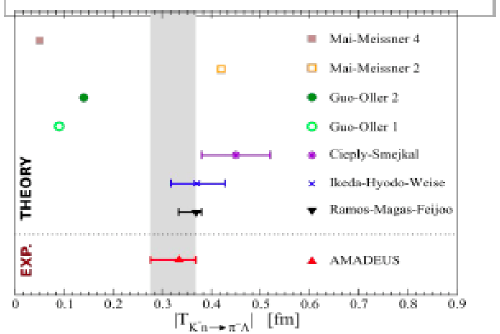

Λ p channel: 2NA, 3NA and 4NA BRs and σ

Process	Branching Ratio (%)	σ (mb)	@	p_K (MeV/c)
2NA-QF Λp	0.25 ± 0.02 (stat.) $^{+0.01}_{-0.02}$ (syst.)	2.8 ± 0.3 (stat.) $^{+0.1}_{-0.2}$ (syst.)	@	128 ± 29
2NA-FSI Λp	6.2 ± 1.4 (stat.) $^{+0.5}_{-0.6}$ (syst.)	69 ± 15 (stat.) ± 6 (syst.)	@	128 ± 29
2NA-QF Σ^0p	0.35 ± 0.09 (stat.) $^{+0.13}_{-0.06}$ (syst.)	3.9 ± 1.0 (stat.) $^{+1.4}_{-0.7}$ (syst.)	@	128 ± 29
2NA-FSI Σ^0p	7.2 ± 2.2 (stat.) $^{+4.2}_{-5.4}$ (syst.)	80 ± 25 (stat.) $^{+46}_{-60}$ (syst.)	@	128 ± 29
2NA-CONV Σ/Λ	2.1 ± 1.2 (stat.) $^{+0.9}_{-0.5}$ (syst.)	-		
3NA Λpn	1.4 ± 0.2 (stat.) $^{+0.1}_{-0.2}$ (syst.)	15 ± 2 (stat.) ± 2 (syst.)	@	117 ± 23
3NA Σ^0pn	3.7 ± 0.4 (stat.) $^{+0.2}_{-0.4}$ (syst.)	41 ± 4 (stat.) $^{+2}_{-5}$ (syst.)	@	117 ± 23
4NA Λpnn	0.13 ± 0.09 (stat.) $^{+0.08}_{-0.07}$ (syst.)	-		
Global Λ(Σ^0)p	21 ± 3 (stat.) $^{+5}_{-6}$ (syst.)	-		

The ratio between the branching ratios of the 2NA-QF in the Λp channel and in the Σ^0p is measured to be:

$$\mathcal{R} = \frac{BR(K^-pp \to \Lambda p)}{BR(K^-pp \to \Sigma^0 p)} = 0.7 \pm 0.2(stat.)^{+0.2}_{-0.3}(syst.)$$

$$\mathrm{BR}(K^-2NA \to YN) = (21.6 \pm 2.9(\mathrm{stat.})^{+4.4}_{-5.6}(\mathrm{syst.}))\%$$

K- p -> $(\Sigma^0/\Lambda)\ \pi^0$

cross section at p_{K^-} = 98 ± 10 MeV/c :

- $\sigma_{K^-p\to\Sigma^0\pi^0} = 42.8 \pm 1.5(stat.)^{+2.4}_{-2.0}(syst.)$ mb
- $\sigma_{K^-p\to\Lambda\pi^0} = 31.0 \pm 0.5(stat.)^{+1.2}_{-1.2}(syst.)$ mb ,

Λ t channel: 4NA BRs and σ

BR(K^{-4}He(4NA) → Λt) < 2.0×10^{-4} /K_{stop} (95% c. l.)
σ(100 ± 19 MeV/c) (K^{-4}He(4NA) → Λt) =
= (0.81 ± 0.21 (stat) $^{+0.03}_{-0.04}$ (syst)) mb

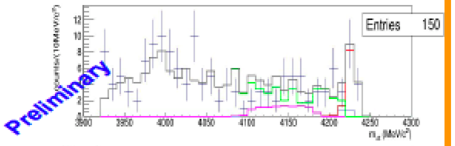

BR(K^{-12}C(4NA) → Λt ^{8}Be) = 1.5 ± 0.5 × 10^{-4} (stat) /K_{stop}
σ(K^{-12}C (4NA) → Λt ^{8}Be) = 0.58 ± 0.11 (stat) mb
σ(K^{-12}C (4NA) → Σ^0t ^{8}Be) = 1.88 ± 0.35 (stat) mb

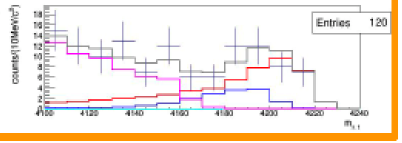

Future perspectives

- The present knowledge of total and differential cross sections of low energy kaon-nucleon reactions is very limited: below 150 MeV/c there is a “desert” - the experimental data are very scarce and with large errors and practically no data exist below 100 MeV/c.
- **Kaon-nucleon scattering/interaction data are fundamental to validate theories; chiral symmetries; lattice calculations; potential models etc.**

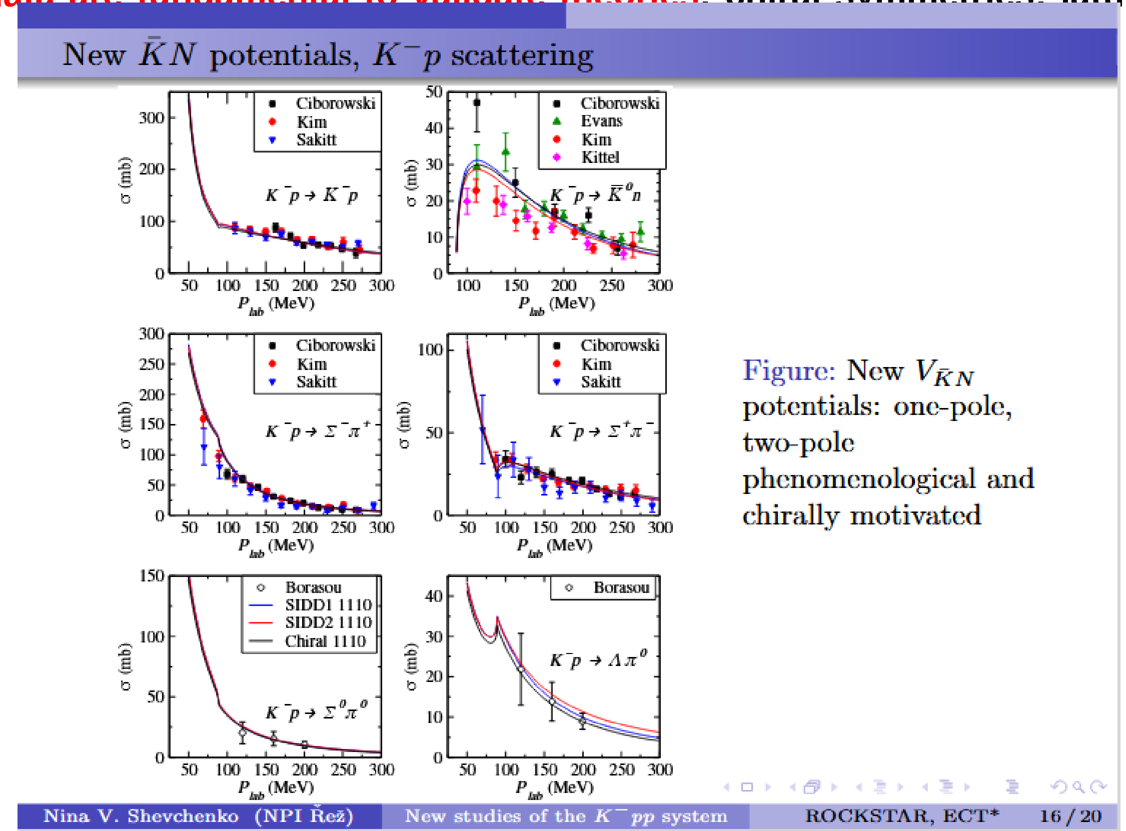

Experiment for kaon-nuclei interaction studies

Charged kaon detector

Cryogenic target:
Solid H2, D2, Ar
Liquid He

Kaon monitor

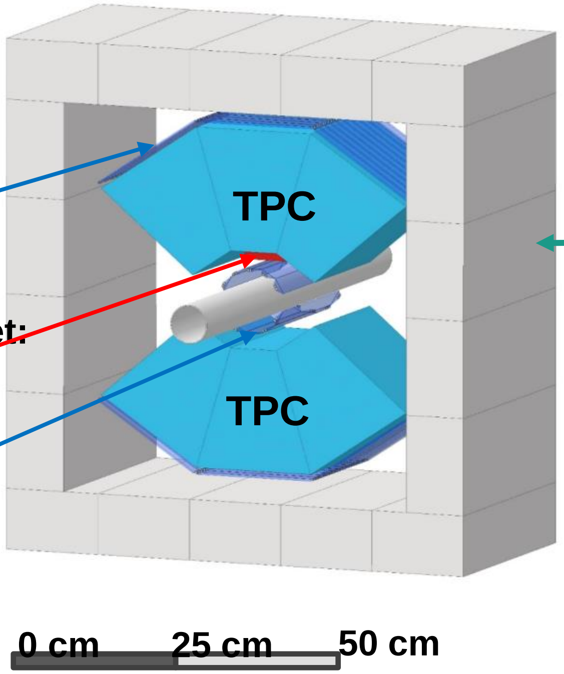

“Sandwich” type calorimeter
32 layers Pb – liq. Scintillator, thickness 25 cm

Thank You

Edgar Allan Poe — 'There is no exquisite beauty… without some strangeness in the proportion.'